International Journal of Thermal Sciences 153 (2020) 106352

Contents lists available at ScienceDirect

International Journal of Thermal Sciences

journal homepage: http://www.elsevier.com/locate/ijts

Semi-analytical thermal modeling of transverse and longitudinal fins in a cylindrical phase change energy storage system

Amirhossein Mostafavi, Mohammad Parhizi, Ankur Jain *

Mechanical and Aerospace Engineering Department, University of Texas at Arlington, Arlington, TX, USA

ARTICLE INFO

Keywords:
Phase change materials
Energy storage
Extended surfaces
Transverse fins
Longitudinal fins
Theoretical modeling

ABSTRACT

Inclusion of fins in phase change energy storage systems has been widely investigated for improving the rate of energy storage. Despite significant past experimental research in this direction, there is a lack of comprehensive theoretical models for fin-based enhancement in energy storage, particularly for cylindrical geometries. This is a considerably challenging, non-linear problem. This paper presents a semi-analytical model for temperature distribution and energy storage in an annular phase change material (PCM) material around a hot cylinder in the presence of transverse and longitudinal fins extending into the PCM. Two distinct pathways for heat transfer into the PCM are analyzed separately and expressions for total heat flux into the PCM are determined for both fin types. The perturbation method is used for analyzing the non-linear phase change problem and determining the heat flux into the PCM through the fin. The dependence of total energy stored on fin thermal properties and geometrical parameters is determined. Results indicate key similarities and differences between cylindrical fins and recently-reported Cartesian fins. It is shown that even a thin fin results in considerable heat transfer enhancement. Results also indicate diminishing results when the fin size is further increased. Theoretical modeling presented in this paper improves the fundamental understanding of an important heat transfer enhancement strategy for phase change based energy storage systems. Results discussed here may help improve the practical design of finned, cylindrical phase change energy storage systems that are commonly used for harnessing renewable energy.

1. Introduction

Renewable energy technologies such as solar energy have been widely investigated in the past to meet the world's energy demand with minimal environmental impact. The unsteady and intermittent nature of renewable energy, however, remains a key challenge. Thermal energy storage (TES) systems can play a vital role in alleviating these challenges by storing and releasing excess renewable energy during periods of availability and demand respectively [1,2].

Thermal energy can be stored using a variety of mechanisms, such as sensible heat [3], latent heat [4] and thermochemical energy [5]. Amongst these, latent heat storage offers advantages of compactness and capability of storing high amount of energy associated with the liquid-to-solid transition of the phase change material (PCM). However, due to the thermal resistance offered by the newly formed phase, the rate of energy storage tends to slow down over time [6]. As a result, enhancing the rate and magnitude of latent energy storage has attracted considerable research [7,8]. A large body of literature exists on possible enhancement mechanisms. Two broad classes of such mechanisms include enhancement of PCM thermal properties through dispersion of nano/micro-particles [9,10] and enhancement of heat transfer into the PCM through extended surfaces such as fins and foams [11,12].

For the case of heat transfer between a hot/cold cylinder of radius R_i and a surrounding annular bed of PCM between $r = R_i$ and $r = R_o$, transverse and longitudinal fins have been commonly used for heat transfer enhancement. These are shown schematically in Fig. 1(a) and (b), respectively. Transverse fins extend throughout circumferentially, with a width w that is lower than the PCM width W in the axial direction. In contrast, longitudinal fins extend through the entire width of the geometry, but are limited to an angle $2\phi_f$ in the circumferential direction. Both fin types have been investigated extensively through experiments and modeling for enhancement of heat transfer into the PCM [13–22]. The effect of number of fins on rate of PCM solidification was numerically and experimentally studied in transverse and longitudinal configurations. It was shown that increase in number of fins decreases solidification time [13,14]. A similar study with constant thickness longitudinal fins reported that 4–5 fins offer optimal performance [15].

* Corresponding author. 500 W First St, Rm 211, Arlington, TX, 76019, USA.
E-mail address: jaina@uta.edu (A. Jain).

https://doi.org/10.1016/j.ijthermalsci.2020.106352
Received 29 August 2019; Received in revised form 29 January 2020; Accepted 26 February 2020

Nomenclature

c	volumetric heat capacity (J/m^{3}K)
$\overline{c}_f$	non-dimensional fin volumetric heat capacity, $\overline{c}_f = \frac{c_f}{c_p}$
H	Length of cylindrical wall (m)
k	thermal conductivity (W/mK)
$\overline{k}_f$	non-dimensional fin thermal conductivity, $\overline{k}_f = \frac{k_f}{k_p}$
L	fin length (m)
L_p	volumetric latent heat of fusion (J/m^3)
N	fin number
q	heat absorbed per unit length (J/m)
$\overline{q}$	non-dimensional heat absorbed, $\overline{q} = \frac{q}{(T_w - T_m)c_p R_i^2}$
q''_{loss}	heat flux from fin into PCM (W/m^2)
Q''	thermal conduction heat flux (W/m^2)
$\overline{S}_a$	non-dimensional source term, $\overline{S}_a = \frac{q''_{loss} R_i}{\phi_f \overline{r}(T_w - T_m)k_f}$
$\overline{S}_r$	non-dimensional source term, $\overline{S}_r = \frac{q''_{loss} R_i}{\overline{w}(T_w - T_m)k_f}$
Ste	Stefan number, $Ste = \frac{c_p(T_w - T_m)}{L_p}$
t	time (s)
$\overline{t}$	non-dimensional time, $\overline{t} = \frac{\alpha_p t}{R_i^2}$
T	temperature (K)
T_m	phase change temperature (K)
T_w	wall temperature (K)
r	spatial coordinate (m)
$\overline{r}$	non-dimensional spatial coordinates, $\overline{r} = \frac{r}{R_i}$
R_i	inner radius (m)
R_o	outer radius (m)
w	width of transverse fin (m)
W	width of the domain for transverse fin (m)
$\overline{w}, \overline{W}$	non-dimensional fin and domain width, $\overline{w} = \frac{w}{R_i}$, $\overline{W} = \frac{W}{R_i}$
z	spatial coordinates (m)
$\overline{z}$	non-dimensional spatial coordinates, $\overline{z} = \frac{z}{R_i}$

Greek symbols

α	thermal diffusivity (m^2/s)
$\overline{\alpha}_f$	non-dimensional fin thermal diffusivity, $\overline{\alpha}_f = \frac{\alpha_f}{\alpha_p}$
β_n	non-dimensional eigenvalues
θ	non-dimensional temperature, $\theta = \frac{T - T_m}{T_w - T_m}$
ϕ	angular coordinate (rad)
φ_f	width of longitudinal fin (rad)
φ_o	width of the domain for longitudinal fin (rad)

Subscripts and superscripts

f	fin
LS	liquid solid interface
p	phase change material
W	wall
*	initial approximation

A numerical study showed overall heat transfer increase with number of fins for a transverse finned storage system [16]. Groulx et al. experimentally investigated melting and solidification in a cylindrical thermal storage system with four longitudinal fins. It was found that solidification process is conduction-dominated throughout, but melting is conduction-dominated only in early stages [17]. The effect of fluid flow rate on melting time in a solar domestic hot water system with longitudinal fins was examined experimentally [18]. The melting time is found to be a strong function of heat transfer fluid flow rate during the charging process, with no effect on the rate of solidification during the discharging process [18]. Measurements have been reported for the effects of heat transfer flow rate and temperature on charging and discharging processes in a finned tube heat exchanger [19]. Ziskind et al. investigated close contact melting (CCM) effects on thermal performance of finned latent heat energy storage enclosures numerically and experimentally. CCM has been reported to improve the melting rate and shorten the melting time by 2.5 times for both transverse and longitudinally finned systems. Similar trend was demonstrated in a helical fined system [20–22]. A numerical study has reported that energy storage increased with decreasing fin pitch and increasing fin length [23].

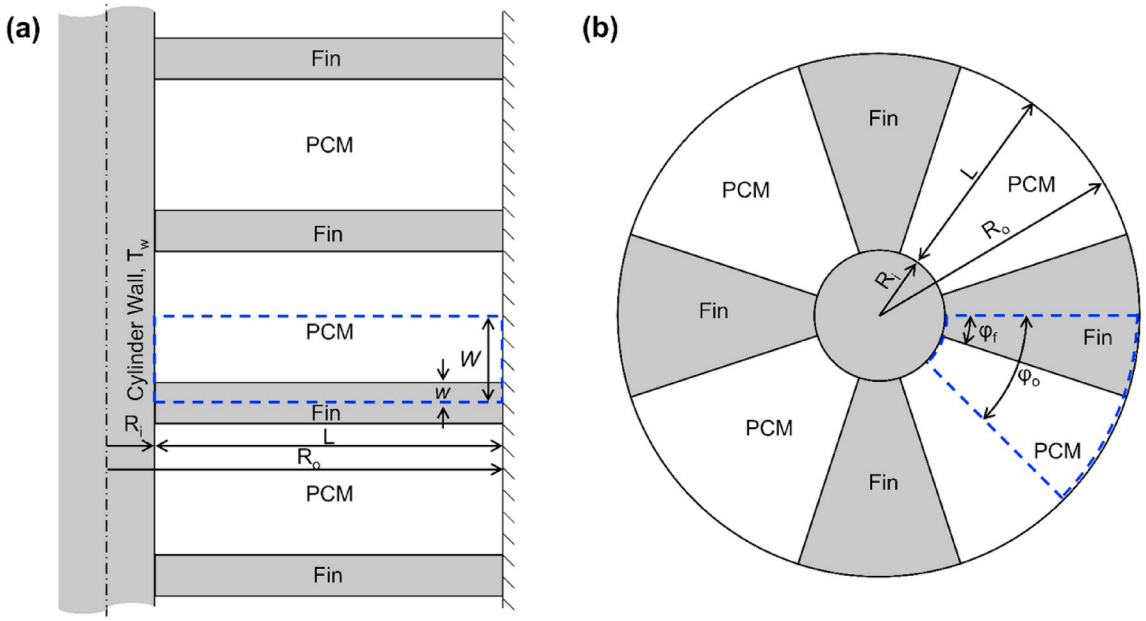

Fig. 1. (a) Schematic cross-section view of multiple transverse fins protruding into an annular PCM bed around a cylindrical heat source; (b) Schematic top view of multiple longitudinal fins protruding into an annular PCM bed around a cylindrical heat source. Unit thermal cells based on symmetry are shown within broken lines for each case.

Another numerical study on energy storage in a transverse finned system showed that the heat storage rate and energy efficiency ratio are largely insensitive to fin geometry when the fin pitch is more than four times the inner radius height and fin length [24]. Using longer and thicker fins improves thermal performance of the system when the fin pitch is small [24]. Effects of length, thickness and number of longitudinal fins on charging and discharging in a triplex tube heat exchanger were investigated numerically by considering pure conduction and natural convection, and the results were validated with experimental results. The effect of length and number of fins on the melting and freezing times was stronger than those of fin thickness [25,26]. An experimental study showed that the effective thermal conductivity of the PCM can be raised by up to three times by using fins in an annular storage system. It is found that fin size and pitch are the key parameters that affect thermal conductivity enhancement [27].

The literature survey presented above shows that optimization of a finned geometry for improving the rate of energy storage is of significant interest. As outlined above, multiple papers have investigated this problem through experiments or numerical simulations for specific geometries. However, there remains a distinct lack of generalized theoretical analysis of this problem for transverse and longitudinal fins. While the presence of a fin may offer extended surface area for heat transfer to the PCM, it also displaces PCM volume that could store energy and reduces the area of direct contact between the PCM and the inner wall. This may not be an important consideration – and fins are not needed at all – if infinite time is available for heat transfer because in such a case, all the PCM will melt eventually. However, for a given finite time window available for heat transfer, which is the case for most practical applications, the analysis of trade-offs between these competing effects is essential for understanding how the fin geometry affects the amount of stored energy. Some research exists on theoretical and numerical analysis of heat transfer in fins in Cartesian systems [28–32]. Past work has shown [28] that a certain fin size – the value of which is a function of fin thermal properties – maximizes the thermal benefit of the fin through a careful balance between the two processes described above. However, there is a lack of similar work for cylindrical phase change energy storage systems. For the specific case of transverse and longitudinal fins shown in Fig. 1(a) and (b), it is of interest to determine how the fin size relative to PCM, w/W and the angle $2\phi_f$ respectively, affect energy storage for a given time duration.

This paper presents analysis of heat transfer into an annular PCM bed from an inner heat source in the presence of transverse or longitudinal fins, with focus on understanding the impact of fin geometry and thermal properties on the amount of energy stored. Governing equations for heat transfer into the PCM, both directly from the wall and through the fins are derived. Sensible and latent heat storage in the PCM are both accounted for. Based on a semi-analytical method, expressions for the total stored energy in the PCM for a given finite time as a function of fin geometry and thermal properties are derived for both transverse and longitudinal fins. Dependence of total stored energy in the PCM on fin size is investigated.

2. Theoretical model

This section develops theoretical models for heat transfer from a constant temperature cylinder into a surrounding, annular PCM bed. Specifically, the effect of two types of fins between the inner and outer radii, R_i and R_o respectively, is captured in these models. As shown in Fig. 1(a), transverse fins go all around circumferentially, with a width w that is lower than the width W of the thermal unit cell. In contrast, as shown in Fig. 1(b), longitudinal fins extend through the entire height of the geometry, but not in the circumferential direction. Given a fixed total number of longitudinal fins, the angular width of each fin $2\phi_f$ is an important design parameter, similar to w for the transverse fins. In general, as w or ϕ_f increases, in the cases of transverse and longitudinal fins, respectively, the area of direct contact between PCM and wall reduces, which inhibits the total amount of direct heat transfer to the PCM in a given total time. However, this also results in greater temperature rise in the fin itself, which provides an additional path for heat transfer into the PCM. Therefore, the effect of w or ϕ_f on overall heat transfer is important to quantify. Note that this is an interesting problem only for a given, finite amount of time available for heat transfer. At infinite time, all of the PCM will melt and reach the wall temperature, and therefore, presence of any fin material is undesirable as it reduces the volume of PCM available and hence the total amount of heat stored.

The next two sub-sections consider geometries with transverse and longitudinal fins, respectively, and derive governing equations for the fin temperature distribution and expressions for the total heat stored in terms of the fin temperature distribution. In each case, the total heat transfer into the PCM is written as the sum of two distinct modes of heat transfer due to two independent, non-overlapping propagation fronts – heat transfer directly from the wall to the PCM, and heat transfer into the PCM indirectly through the fin.

2.1. Transverse fin

In this case, transverse fins extending throughout the circumferential direction and between $r = R_i$ to $r = R_o$ in the radial direction are considered. The fin pitch and fin width in the axial direction are taken to be $2W$ and $2w$, respectively, so that heat transfer analysis can be simplified by modeling an axisymmetric unit cell, as shown in Fig. 2(a). Both fin and PCM are assumed to be at PCM melting temperature T_m initially. Note that k and c denote thermal conductivity and volumetric heat capacity, respectively. Subscripts f and p denote fin and PCM, respectively. L_p represents latent heat of PCM. All properties are assumed to be independent of temperature. Total heat absorbed by the PCM up to time, t, $q(t)$ comprises two distinct components –heat absorbed by the PCM directly from the width $(W\text{-}w)$ of the heat source, $q_1(t)$, and heat absorbed by the PCM from the fin, $q_2(t)$.

These components are shown in Fig. 2(a). The first component, $q_1(t)$, depends only on the cylinder temperature $(T_w\text{-}T_m)$ and PCM properties. On the other hand, the second component, $q_2(t)$, depends additionally on fin properties because it is governed by the extent of thermal diffusion into the fin. $q_1(t)$ and $q_2(t)$ independently initiate and propagate melting fronts in r and z directions, respectively. Neglecting the small region near the origin where these two fronts merge, one may determine $q_1(t)$ and $q_2(t)$ independently. Such a simplifying assumption of independent phase change fronts is commonly made to simplify two-dimensional phase change problems [28,29,33]. Expressions for $q_1(t)$ and $q_2(t)$ are now derived separately.

2.1.1. $q_1(t)$ for transverse fin

The $q_1(t)$ component can be determined by solving the problem of phase change propagation into an infinite PCM from a constant temperature cylinder of radius R_i. While similar to the classical Stefan problem in Cartesian coordinates, this problem does not appear to have an exact analytical solution. Parhizi & Jain [34] have presented a solution for this problem based on perturbation method. Referring to the non-dimensionalization summarized in the Nomenclature section, the location of the solid-liquid interface location, $\bar{r}_{LS}$ as a function of non-dimensional time $\bar{t}$ is given by the following inverse relationship

$$\bar{t} = \left[\frac{(2(\bar{r}_{LS}(\bar{t}))^2 \log\bar{r}_{LS}(\bar{t}) + 1)}{4} + \frac{Ste}{4\log\bar{r}_{LS}(\bar{t})}\left((\bar{r}_{LS}(\bar{t}))^2 \log\bar{r}_{LS}(\bar{t}) + \log\bar{r}_{LS}(\bar{t}) - (\bar{r}_{LS}(\bar{t}))^2 + 1\right) + \frac{Ste^2}{128(\bar{r}_{LS}(\bar{t}))^2 \log\bar{r}_{LS}(\bar{t})}\left((\bar{r}_{LS}(\bar{t}))^4\left(8(\log\bar{r}_{LS}(\bar{t}))^3 - 20(\log\bar{r}_{LS}(\bar{t}))^2 + 21\log\bar{r}_{LS}(\bar{t}) - 8\right) - 16(\bar{r}_{LS}(\bar{t}))^2(\log\bar{r}_{LS}(\bar{t}) - 1) - 5\log\bar{r}_{LS}(\bar{t}) - 8\right)\right] \quad (1)$$

Consequently, the total heat absorbed by the PCM directly from the

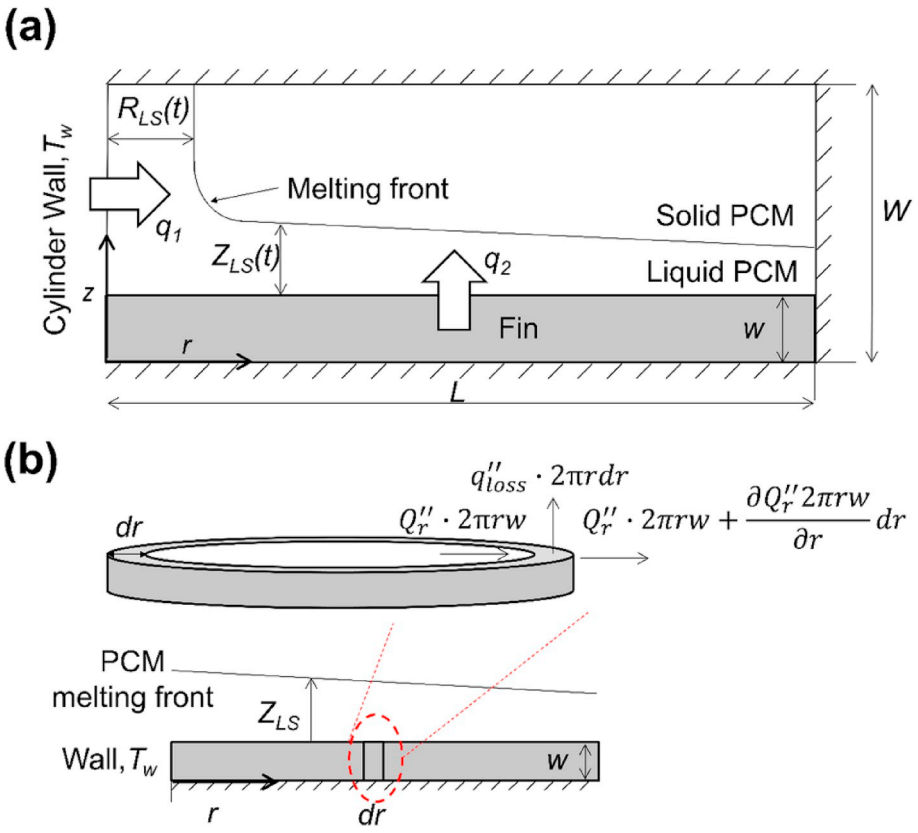

Fig. 2. (a) Schematic of two melting fronts within the unit cell for transverse fin thermal analysis; (b) Schematic of an infinitesimal fin element for deriving governing energy conservation equation for temperature distribution in transverse fin.

cylinder wall, $q_1(t)$, considering the reduced area of direct contact due to the presence of the fin, as shown in Fig. 2(a), is given by differentiating the temperature distribution in the PCM at the interface $r = R_i$ [34]. The final result is

$$\begin{aligned}
&\bar{q}_1(\bar{t}) = -2\left(1-\frac{\overline{w}}{\overline{W}}\right)\int_0^{\bar{t}}\left(\frac{\partial\theta_p}{\partial\bar{r}}\right)_{\bar{r}=\bar{R}_i}\\
&d\bar{t} = \int_0^{\bar{t}} -2\left(1-\frac{\overline{w}}{\overline{W}}\right)\left(\left(\frac{(10(\bar{r}_{LS}(\bar{t}))^4+8(\bar{r}_{LS}(\bar{t}))^2-6)}{64(\bar{r}_{LS}(\bar{t}))^4(\log\bar{r}_{LS}(\bar{t}))^4}\right.\right.\\
&-\frac{(5(\bar{r}_{LS}(\bar{t}))^2-1)^2}{16(\bar{r}_{LS}(\bar{t}))^4(\log\bar{r}_{LS}(\bar{t}))^7}-\frac{(56(\bar{r}_{LS}(\bar{t}))^4+24(\bar{r}_{LS}(\bar{t}))^2+44)}{128(\bar{r}_{LS}(\bar{t}))^4(\log\bar{r}_{LS}(\bar{t}))^5}\\
&\left.+\frac{((\bar{r}_{LS}(\bar{t}))^2-1)(71(\bar{r}_{LS}(\bar{t}))^2+71)}{128(\bar{r}_{LS}(\bar{t}))^4(\log\bar{r}_{LS}(\bar{t}))^6}\right)Ste^2\\
&+\left(\frac{((\bar{r}_{LS}(\bar{t}))^2-1)}{4(\bar{r}_{LS}(\bar{t}))^2(log\bar{r}_{LS}(\bar{t}))^4}-\frac{((\bar{r}_{LS}(\bar{t}))^2+1)}{4(\bar{r}_{LS}(\bar{t}))^2(\log\bar{r}_{LS}(\bar{t}))^3}\right)Ste-\frac{1}{\log\bar{r}_{LS}(\bar{t})}\Bigg)d\bar{t}
\end{aligned} \tag{2}$$

2.1.2. $q_2(t)$ for transverse fin

The second pathway for heat transfer into the PCM is through the fin. Since the fin itself is at the melting temperature initially and only heats up over time due to transient thermal diffusion, this is a more complicated problem than $q_1(t)$. In this case, $q_2(t)$ depends on the fin temperature distribution $\theta_f(\bar{r},\bar{t})$. In addition to axisymmetry, the fin is also assumed to have no thermal gradient in the axial direction, which is justified by the thin nature of the fin compared to its length. In such a case, as shown in Fig. 2(b), energy balance of an infinitesimal element of the fin with width w and radial size dr is considered. In addition to thermal conduction into and out of this element, heat loss to the PCM occurs from the top surface. Using Fourier's law, energy balance for this element can be used to derive a governing partial differential equation for the fin temperature

$$\frac{\bar{c}_f}{\bar{k}_f}\frac{\partial\theta_f}{\partial\bar{t}} = \frac{1}{\bar{r}}\frac{\partial}{\partial\bar{r}}\left(\bar{r}\frac{\partial\theta_f}{\partial\bar{r}}\right) - \bar{S}_r \tag{3}$$

where $\bar{S}_r$ represents heat loss to the surrounding PCM. $\bar{S}_r$ is related to the gradient of the PCM temperature distribution $\theta_p(\bar{r},\bar{t})$ at the wall. Therefore, $\theta_p(\bar{r},\bar{t})$ must be determined in order to proceed. Recognizing that the fin temperature itself changes over time, this is a problem of one-dimensional phase change propagation from a wall with time-dependent wall temperature. A solution for this problem is available based on perturbation method [35,36]. The PCM temperature can be written as a power series involving the Stefan number.

$$\theta_p(\bar{r},\bar{z},\bar{t}) = \theta_0(\bar{r},\bar{z},\bar{t}) + Ste\cdot\theta_1(\bar{r},\bar{z},\bar{t}) + (Ste)^2\cdot\theta_2(\bar{r},\bar{z},\bar{t}) \tag{4}$$

where θ_0, θ_1 and θ_2 can be shown to be functions of the fin temperature distribution as follows

$$\theta_0(\bar{r},\bar{z},\bar{t}) = \theta_f\left(1-\frac{\bar{z}}{\bar{z}_{LS}}\right) \tag{5}$$

$$\theta_1(\bar{r},\bar{z},\bar{t}) = \frac{1}{6}\theta_f\left(\frac{\bar{z}}{\bar{z}_{LS}}\right)\left(\frac{\bar{z}}{\bar{z}_{LS}}-1\right)\left[\theta_f\left(\frac{\bar{z}}{\bar{z}_{LS}}+1\right)-\frac{\dot{\theta_f}}{\dot{\bar{z}}_{LS}}\bar{z}_{LS}\left(\frac{\bar{z}}{\bar{z}_{LS}}-2\right)\right] \tag{6}$$

$$\begin{aligned}
\theta_2(\bar{r},\bar{z},\bar{t}) = &-\frac{1}{360}\theta_f\left(\frac{\bar{z}}{\bar{z}_{LS}}\right)\left(\frac{\bar{z}}{\bar{z}_{LS}}-1\right)\left[\theta_f^2\left(\frac{\bar{z}}{\bar{z}_{LS}}+1\right)\left(9\left(\frac{\bar{z}}{\bar{z}_{LS}}\right)^2+19\right)\right.\\
&\left.+10\left(\frac{\dot{\theta_f}}{\dot{\bar{z}}_{LS}}\right)^2\bar{z}_{LS}^2\left(\frac{\bar{z}}{\bar{z}_{LS}}+4\right)+5\theta_f\frac{\dot{\theta_f}}{\dot{\bar{z}}_{LS}}\bar{z}_{LS}\left(3\left(\frac{\bar{z}}{\bar{z}_{LS}}\right)^2+5\left(\frac{\bar{z}}{\bar{z}_{LS}}\right)+17\right)\right]
\end{aligned} \tag{7}$$

As a result, an expression for $\bar{S}_r$ in equation (3) can be written as

$$\overline{S}_r = \frac{1}{\overline{k}_f \overline{w}} \left[\frac{\theta_f}{\overline{z}_{LS}} + Ste \frac{\theta_f \left(\theta_f + 2 \frac{\dot{\theta}_f}{\dot{\overline{z}}_{LS}} \overline{z}_{LS} \right)}{6 \overline{z}_{LS}} - \frac{\theta_f \left(40 \left(\frac{\dot{\theta}_f}{\dot{\overline{z}}_{LS}} \right)^2 \overline{z}_{LS}^2 + 85 \theta_f \frac{\dot{\theta}_f}{\dot{\overline{z}}_{LS}} \overline{z}_{LS} + 19 \theta_f^2 \right)}{(Ste)^2 360 \overline{z}_{LS}} \right] \tag{8}$$

where the location of the melting front originating from the transverse fin surface, $\overline{z}_{LS}$ is given by [35,36].

$$\overline{z}_{LS}(\overline{r}, \overline{t}) = \left[2Ste \int_0^{\overline{t}} \theta_f(\overline{r}, \overline{\tau}) \left(1 - \frac{Ste}{3} \theta_f(\overline{r}, \overline{\tau}) + \frac{7}{45} (Ste)^2 \theta_f(\overline{r}, \overline{\tau})^2 \right) d\overline{\tau} \right]^{\frac{1}{2}} \tag{9}$$

Note the primes in equations (6)–(8) represent derivatives with respect to time. Equations (8) and (9) determine heat loss from a given radial location on transverse fin surface at any given time in terms of the prior fin temperature history at that location and PCM thermal properties.

A complete partial differential equation in $\theta_f(\overline{r}, \overline{t})$ can be derived by combining equations (3) and (8) as

$$\frac{\overline{c}_f}{\overline{k}_f} \frac{\partial \theta_f}{\partial \overline{t}} = \frac{1}{\overline{r}} \frac{\partial}{\partial \overline{r}} \left(\overline{r} \frac{\partial \theta_f}{\partial \overline{r}} \right) - \frac{1}{\overline{k}_f \overline{w}} \left[\frac{\theta_f}{\overline{z}_{LS}} + Ste \frac{\theta_f \left(\theta_f + 2 \frac{\dot{\theta}_f}{\dot{\overline{z}}_{LS}} \overline{z}_{LS} \right)}{6 \overline{z}_{LS}} - \frac{\theta_f \left(40 \left(\frac{\dot{\theta}_f}{\dot{\overline{z}}_{LS}} \right)^2 \overline{z}_{LS}^2 + 85 \theta_f \frac{\dot{\theta}_f}{\dot{\overline{z}}_{LS}} \overline{z}_{LS} + 19 \theta_f^2 \right)}{(Ste)^2 360 \overline{z}_{LS}} \right] \tag{10}$$

Boundary and initial conditions associated with equation (10) must be defined. The fin temperature equals the cylinder wall temperature at fin base, $\overline{r} = 1$. Adiabatic boundary condition applies at fin tip, $\overline{r} = \frac{R_o}{R_i}$. Finally, the fin temperature $\theta_f(\overline{r}, 0)$ is 0 initially. Equations (11)–(13) express these requirements mathematically:

$$\theta_f(1, \overline{t}) = 1 \tag{11}$$

$$\left(\frac{\partial \theta_f}{\partial \overline{r}} \right)_{\overline{r} = \overline{R}_0} = 0 \tag{12}$$

$$\theta_f(\overline{r}, 0) = 0 \tag{13}$$

Equation (10) contains only the fin temperature and is uncoupled from the PCM temperature. In principle, a solution of equation (10) can be used to determine $\overline{q}_2(\overline{t})$, the total heat flux into the PCM from the fin surface as follows

$$\overline{q}_2(\overline{t}) = \frac{2}{\overline{W}} \int_0^{\overline{t}} \int_{\overline{R}_i}^{\overline{R}_o} \left(\frac{\partial \theta_p}{\partial \overline{z}} \right)_{\overline{z}=0}$$

$$\overline{r} d\overline{r} d\overline{t} = \frac{2}{\overline{W}} \int_0^{\overline{t}} \int_{\overline{R}_i}^{\overline{R}_o} \left[\frac{\theta_f}{\overline{z}_{LS}} + Ste \frac{\theta_f \left(\theta_f + 2 \frac{\dot{\theta}_f}{\dot{\overline{z}}_{LS}} \overline{z}_{LS} \right)}{6 \overline{z}_{LS}} - \frac{\theta_f \left(40 \left(\frac{\dot{\theta}_f}{\dot{\overline{z}}_{LS}} \right)^2 \overline{z}_{LS}^2 + 85 \theta_f \frac{\dot{\theta}_f}{\dot{\overline{z}}_{LS}} \overline{z}_{LS} + 19 \theta_f^2 \right)}{(Ste)^2 360 \overline{z}_{LS}} \right] \overline{r} d\overline{r} d\overline{t} \tag{14}$$

However, it is very challenging to solve equation (10) explicitly due to the complicated and non-linear nature of the source term. A time-stepping approach for solving equation (10) is discussed in section 2.3.

Heat transfer analysis of a longitudinal fin is discussed next.

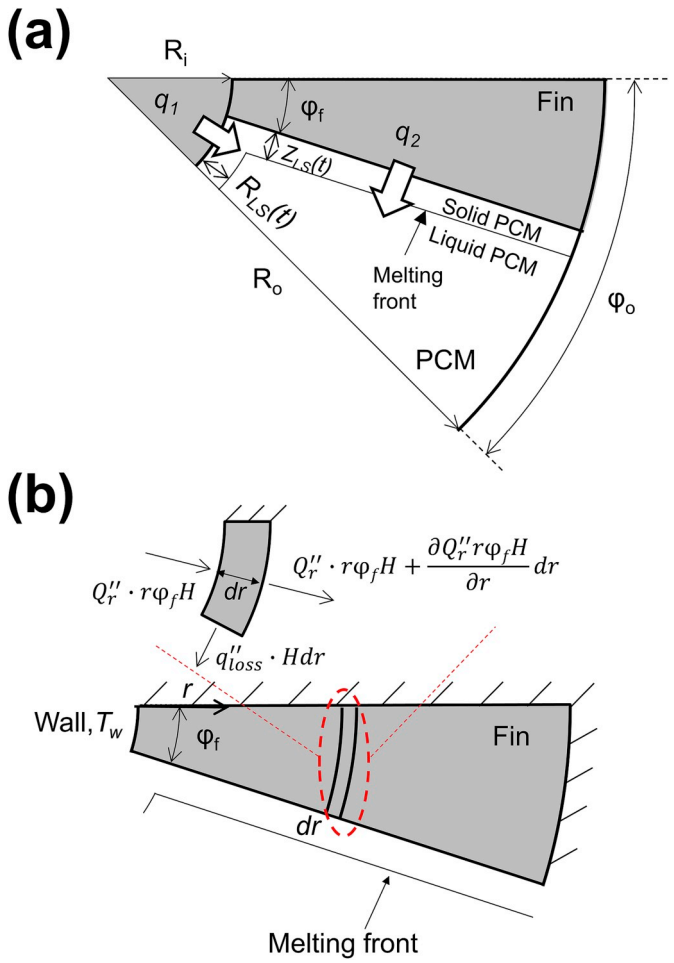

Fig. 3. (a) Schematic of two melting fronts within the unit cell for longitudinal fin thermal analysis; (b) Schematic of an infinitesimal fin element for deriving governing energy conservation equation for temperature distribution in longitudinal fin.

2.2. Longitudinal fin

This sub-section considers longitudinal fins that extend through the axial coordinate, but not in the circumferential direction, as shown in the top view in Fig. 1(b). The number of fins is assumed to be constant and distributed evenly around the periphery of the cylinder, so that the angle ϕ_o in Fig. 1(b) is fixed. Based on symmetry in the problem, the unit cell in the circumferential direction that can be considered for analysis denoted in Fig. 1(b) and shown in detail in Fig. 3(a). Similar to the traverse fin analysis, it is assumed that fin temperature distribution is one dimensional, in this case, radial. This is a reasonable assumption when fin width $\phi_f \cdot R_o$ is small compared to the fin length R_o-R_i.

The goal of analysis presented in this section is to determine the effect of fin size ϕ_f on the total heat absorbed by the PCM in a given time. Similar to the transverse fins considered in section 2.1, there may be a distinct trade-off here between reduced area of direct PCM-cylinder contact and greater thermal conduction into the fin as a result of increasing the fin size. The specific nature of the trade-off, of course, depends on the various non-dimensional parameters that govern the problem, and must be carefully analyzed through modeling.

Similar to the case of transverse fins, the two components of heat transfer into the PCM are evaluated next.

2.2.1. $q_1(t)$ for longitudinal fins

Analysis for determining the heat transfer directly from the cylinder to the PCM can be carried out using the one-dimensional Stefan problem

with constant wall temperature, similar to the transverse fin case in section 2.1.1, with the only difference being the base area. In this case, $\overline{q}_1(\bar{t})$ is given by:

$$\overline{q}_1(\bar{t}) = \left(\frac{\phi_f}{\pi} - \frac{1}{N}\right)\int_0^{\bar{t}} \left(\frac{\partial \theta_p}{\partial \bar{r}}\right)_{\bar{r}=\overline{R}_i} d\bar{t} = \int_0^{\bar{t}} \left(\frac{\phi_f}{\pi} - \frac{1}{N}\right) \left(\left(\frac{(10(\bar{r}_{LS}(\bar{t}))^4 + 8(\bar{r}_{LS}(\bar{t}))^2 - 6)}{64(\bar{r}_{LS}(\bar{t}))^4(\log \bar{r}_{LS}(\bar{t}))^4} - \frac{(5(\bar{r}_{LS}(\bar{t}))^2 - 1)^2}{16(\bar{r}_{LS}(\bar{t}))^4(\log \bar{r}_{LS}(\bar{t}))^7} - \frac{(56(\bar{r}_{LS}(\bar{t}))^4 + 24(\bar{r}_{LS}(\bar{t}))^2 + 44)}{128(\bar{r}_{LS}(\bar{t}))^4(\log \bar{r}_{LS}(\bar{t}))^5} + \frac{((\bar{r}_{LS}(\bar{t}))^2 - 1)(71(\bar{r}_{LS}(\bar{t}))^2 + 71)}{128(\bar{r}_{LS}(\bar{t}))^4(\log \bar{r}_{LS}(\bar{t}))^6}\right) Ste^2 + \left(\frac{((\bar{r}_{LS}(\bar{t}))^2 - 1)}{4(\bar{r}_{LS}(\bar{t}))^2(\log \bar{r}_{LS}(\bar{t}))^4} - \frac{((\bar{r}_{LS}(\bar{t}))^2 + 1)}{4(\bar{r}_{LS}(\bar{t}))^2(\log \bar{r}_{LS}(\bar{t}))^3}\right) Ste - \frac{1}{\log \bar{r}_{LS}(\bar{t})}\right) d\bar{t} \tag{15}$$

where N is the total number of fins in the circumferential direction. N is assumed to be fixed in this analysis.

2.2.2. $q_2(t)$ for longitudinal fins

Analysis for determining the heat transfer into PCM through a longitudinal fin is also similar to the transverse fin case presented in section 2.1.2, but with some key differences. Mainly, the infinitesimal element to be considered for deriving the partial differential equation for the temperature distribution $\theta_f(\bar{r}, \bar{t})$ has a different shape . Unlike the previous case, this element now subtends in the circumferential direction, as shown in Fig. 3(b). Assuming thermal uniformity in the circumferential direction, which is valid as long as $\phi_f \cdot R_o$ is smaller than fin size R_o-R_i, the governing energy conservation equation can be written as

$$\frac{\overline{c}_f}{\overline{k}_f}\frac{\partial \theta_f}{\partial \bar{t}} = \frac{1}{\bar{r}}\frac{\partial}{\partial \bar{r}}\left(\bar{r}\frac{\partial \theta_f}{\partial \bar{r}}\right) - \overline{S}_a \tag{16}$$

where $\overline{S}_a$ accounts for heat loss into the PCM.

Similar to the transverse fin case, $\overline{S}_a$ can be determined by accounting for phase change propagation into the PCM due to time-dependent temperature boundary condition at the fin base. A key difference is the area of contact between the fin element and PCM. Using the temperature solution based on perturbation method, an expression for $\overline{S}_a$ can be derived as

$$\overline{S}_a = \frac{1}{\overline{k}_f \bar{r}\phi_f}\left[\frac{\theta_f}{\overline{z}_{LS}} + Ste\frac{\theta_f\left(\theta_f + 2\frac{\dot{\theta_f}}{\dot{\overline{z}}_{LS}}\overline{z}_{LS}\right)}{6\overline{z}_{LS}} - (Ste)^2\frac{\theta_f\left(40\left(\frac{\dot{\theta_f}}{\dot{\overline{z}}_{LS}}\right)^2\overline{z}_{LS}^2 + 85\theta_f\frac{\dot{\theta_f}}{\dot{\overline{z}}_{LS}}\overline{z}_{LS} + 19\theta_f^2\right)}{360\overline{z}_{LS}}\right] \tag{17}$$

This assumes that melting front location $\overline{z}_{LS}$, derived by equation (9) for transverse fins can also be used for longitudinal fins in the circumferential direction. This is a reasonable assumption as long as the fin angle ϕ_f is small.

Combining equations (16) and (17), a partial differential equation for the fin temperature distribution may be derived as

$$\frac{\overline{c}_f}{\overline{k}_f}\frac{\partial \theta_f}{\partial \bar{t}} = \frac{1}{\bar{r}}\frac{\partial}{\partial \bar{r}}\left(\bar{r}\frac{\partial \theta_f}{\partial \bar{r}}\right) - \frac{1}{\overline{k}_f \bar{r}\phi_f}\left[\frac{\theta_f}{\overline{z}_{LS}} + Ste\frac{\theta_f\left(\theta_f + 2\frac{\dot{\theta_f}}{\dot{\overline{z}}_{LS}}\overline{z}_{LS}\right)}{6\overline{z}_{LS}} - (Ste)^2\frac{\theta_f\left(40\left(\frac{\dot{\theta_f}}{\dot{\overline{z}}_{LS}}\right)^2\overline{z}_{LS}^2 + 85\theta_f\frac{\dot{\theta_f}}{\dot{\overline{z}}_{LS}}\overline{z}_{LS} + 19\theta_f^2\right)}{360\overline{z}_{LS}}\right] \tag{18}$$

Following the determination of the fin temperature distribution from equation (18), the heat loss into the PCM, $q_2(t)$ can be written as

$$\overline{q}_2(\bar{t}) = \frac{1}{\pi}\int_0^{\bar{t}}\int_{\overline{R}_i}^{\overline{R}_o}\left(\frac{\partial \theta_p}{\partial \bar{z}}\right)_{\bar{z}=0} d\bar{r}d\bar{t} = \frac{1}{\pi}\int_0^{\bar{t}}\int_{\overline{R}_i}^{\overline{R}_o}\left[\frac{\theta_f}{\overline{z}_{LS}} + Ste\frac{\theta_f\left(\theta_f + 2\frac{\dot{\theta_f}}{\dot{\overline{z}}_{LS}}\overline{z}_{LS}\right)}{6\overline{z}_{LS}} - (Ste)^2\frac{\theta_f\left(40\left(\frac{\dot{\theta_f}}{\dot{\overline{z}}_{LS}}\right)^2\overline{z}_{LS}^2 + 85\theta_f\frac{\dot{\theta_f}}{\dot{\overline{z}}_{LS}}\overline{z}_{LS} + 19\theta_f^2\right)}{360\overline{z}_{LS}}\right] d\bar{r}d\bar{t} \tag{19}$$

This completes the derivation of the two components of heat transfer into the PCM for the longitudinal fin.

Calculation of total heat transfer into the PCM requires determination of the fin temperature distribution by solving the governing energy equation, which in both cases discussed above, are complicated partial differential equations. Since an analytical solution for these equations is unlikely, a timestepping approach for evaluating the temperature distribution is discussed in the next section.

2.3. Timestepping approach for determining fin temperature distribution

While difficult to solve exactly equations (10) and (18) are quite amenable to numerical computation based timestepping. A key challenge, similar to Cartesian fins [28], is the singularity at $\bar{t} = 0$ in the source terms, which results in difficulties in the initial timestepping. An approximation is made in order to overcome this challenge. Heat transfer into the fin from $\bar{t} = 0$ up to a small time $\bar{t}^*$ is assumed to occur without heat loss into the PCM. This may be a reasonable approximation for small values of $\bar{t}^*$, up to which, the propagation of phase change front, and hence the area of contact between the fin and PCM is small. This is a helpful approximation because neglecting heat loss to the PCM in equations (10) and (18) reduces these equations to standard thermal conduction problems, which can be solved to provide temperature distribution in the fin at $\bar{t} = \bar{t}^*$. Following this, the timestepping approach, including the effect of heat loss to the PCM can be carried out, because there is no singularity in the governing equation for $\bar{t} > 0$. The value of $\bar{t}^*$ clearly needs to be chosen to be small enough to minimize the error involved in neglecting heat transfer to the PCM up to $\bar{t} = \bar{t}^*$.

Based on the assumption of neglecting heat transfer into the PCM, analytical expressions for fin temperature distribution at $\bar{t} = \bar{t}^*$ can be determined by using the method of separation of variables. For both transverse and longitudinal fins, the result is

$$\theta_f^*(\bar{r}, \bar{t}^*) = 1 - 2\sum_{n=1}^{\infty}\exp\left(-\frac{\beta_n^2}{\overline{R}_o^2}\bar{t}^*\right)\frac{Y_1(\beta_n)J_0\left(\beta_n\frac{\bar{r}}{\overline{R}_o}\right) - J_1(\beta_n)Y_0\left(\beta_n\frac{\bar{r}}{\overline{R}_o}\right)}{C_n} \tag{20}$$

where

$$C_n = \beta_n\left[\left(Y_0(\beta_n)J_0\left(\frac{\beta_n}{\overline{R}_o}\right) - J_0(\beta_n)Y_0\left(\frac{\beta_n}{\overline{R}_o}\right)\right) - \frac{1}{\overline{R}_o}\left(Y_1(\beta_n)J_1\left(\frac{\beta_n}{\overline{R}_o}\right) - J_1(\beta_n)Y_1\left(\frac{\beta_n}{\overline{R}_o}\right)\right)\right] \tag{21}$$

and β_n are roots of the transcendental equation

$$Y_1(x)J_0\left(\frac{x}{\overline{R}_o}\right) - J_1(x)Y_0\left(\frac{x}{\overline{R}_o}\right) = 0 \tag{22}$$

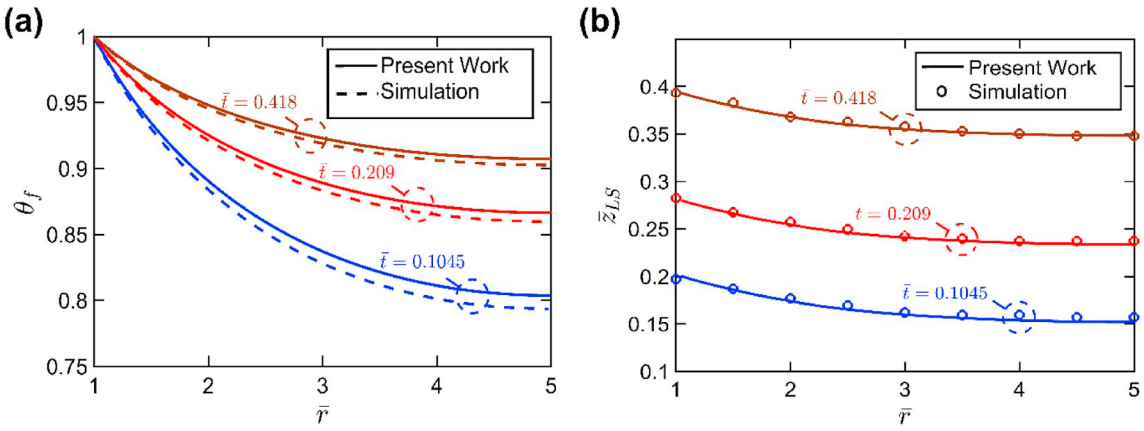

Fig. 4. Validation of theoretical models by comparison with finite-element simulations: (a) Temperature distribution and (b) phase change front location at multiple times for a transverse fin with $\overline{W} = 2$, $\overline{w} = 0.5$, $\overline{L} = 4$, Ste $= 0.19$, $\overline{k}_f = 1580$, $\overline{c}_f = 1.36$.

3. Results and discussion

3.1. Model validation

Comparison with finite element simulation is first carried out in ANSYS-CFX to validate the analytical models presented in section 2. In this case, the system presented in Fig. 2(a) is considered with aluminum transverse fin and octadecane PCM. Melting point, density, heat capacity, thermal conductivity and latent heat of the PCM are taken to be 28 °C, 780 kg/m^3, 2300 J/kgK, 0.15 W/mK and 244,000 J/kg, respectively, corresponding to properties of octadecane, a commonly used PCM [37]. Standard thermal properties are assumed for aluminum. Temperature of the inner wall is maintained at 20 K above the phase change temperature of the PCM.

The finite-element simulation determines the fin and PCM temperature distributions as well as the phase change propagation using the enthalpy method, where the PCM is defined as a homogenous binary mixture of solid and liquid phases. The PCM is assumed to initially be completely solid. The quadrilateral/triangular mesh in the simulation is swept in circumferential and axial directions for transverse and longitudinal fin configurations respectively. Grid independence analysis is carried out to show that variation in predicted temperature is negligible beyond 232,128 and 696,384 nodes in the fin and PCM, respectively.

Fig. 4(a) shows a comparison of predicted fin temperature distribution between the model presented in section 2.1 and the finite element simulation at multiples times. In addition, comparison of the phase change interface location computed with analytical model and the finite element simulation is shown in Fig. 4(b). There is good agreement between the analytical model and finite element simulation for both temperature distribution and phase change interface. The worst-case deviation between the analytical model and finite-element simulation is 1.2% and 3.5% for data shown in Fig. 4(a) and (b), respectively. Note that in this case, a small value of $\bar{t}^* = 2.09 \times 10^{-4}$, equivalent to 0.05% of the total time is used. A small value of $\bar{t}^*$ is needed to minimize error due to the initial approximation.

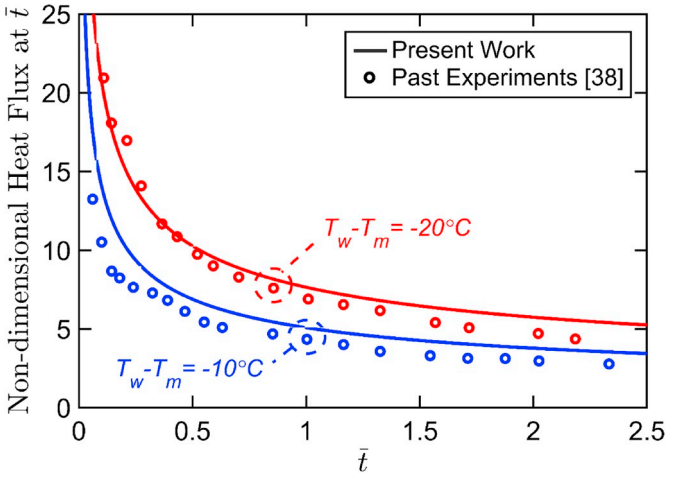

Fig. 5. Validation of the analytical model by comparison of predicted heat flux as a function of time with past experimental measurements [38] for solidification of n-Eicosane with four fins around a cold, 45 mm diameter cylinder for two different wall temperatures.

In addition, the analytical model presented in this work is also compared with experimental data reported by Sasaguchi et al. [38]. Fig. 5 plots non-dimensional heat flux as a function of time and compares the analytical model and past experimental data for solidification of n-Eicosane contained in an annular region around a cold inner cylinder wall with four longitudinal fins. Fig. 5 carries out this comparison for two different wall temperatures for which Sasguchi et al. [38] reported measurements. Thermal properties of the PCM and fin are taken from the past work [38]. Non-dimensionalization is carried out similar to other results in the present work. Fig. 5 shows good agreement between the present analytical model and the past experimental work for both cases, thereby providing additional validation of the present work. Please note that the present work ignores convective heat transfer effects and assumes constant thermal properties, which may contribute to the small disagreement between modeling and measurements. Further, the fins used by Sasaguchi et al. appear to have constant thickness, whereas the fin thickness in the present work increases radially outwards, which may also be a source of disagreement between the two.

3.2. Effect of fin size on heat stored

Total heat transfer into the PCM in a transverse finned system, $\overline{q}_t$, along with its two components $\overline{q}_1$ and $\overline{q}_2$ are shown in Fig. 6(a)–(f) as a function of $\overline{w}/\overline{W}$ for six different values of fin thermal conductivity $\overline{k}_f$. The total time is $\bar{t} = 0.418$. $\overline{q}_1$ and $\overline{q}_2$ are calculated by equations (2) and (14), respectively. For comparison, the total heat stored in the absence of fins is 4.98 in non-dimensional form. Fig. 6 shows that as $\overline{w}/\overline{W}$increases, heat transfer from fin surface into the PCM, $\overline{q}_2$, improves due to greater thermal diffusion into the fin. As a result, $\overline{q}_2$ increases sharply with $\frac{\overline{w}}{\overline{W}}$ for small values of $\frac{\overline{w}}{\overline{W}}$, but saturates at larger values. On the other hand, a higher value of $\overline{w}/\overline{W}$ results in lower area of direct contact between the wall and the PCM. This contributes to reduced heat transfer from the wall into the PCM, $\overline{q}_1$, as seen in Fig. 6(a)–(f). For any given fin thermal conductivity, total heat absorbed by the PCM, given by

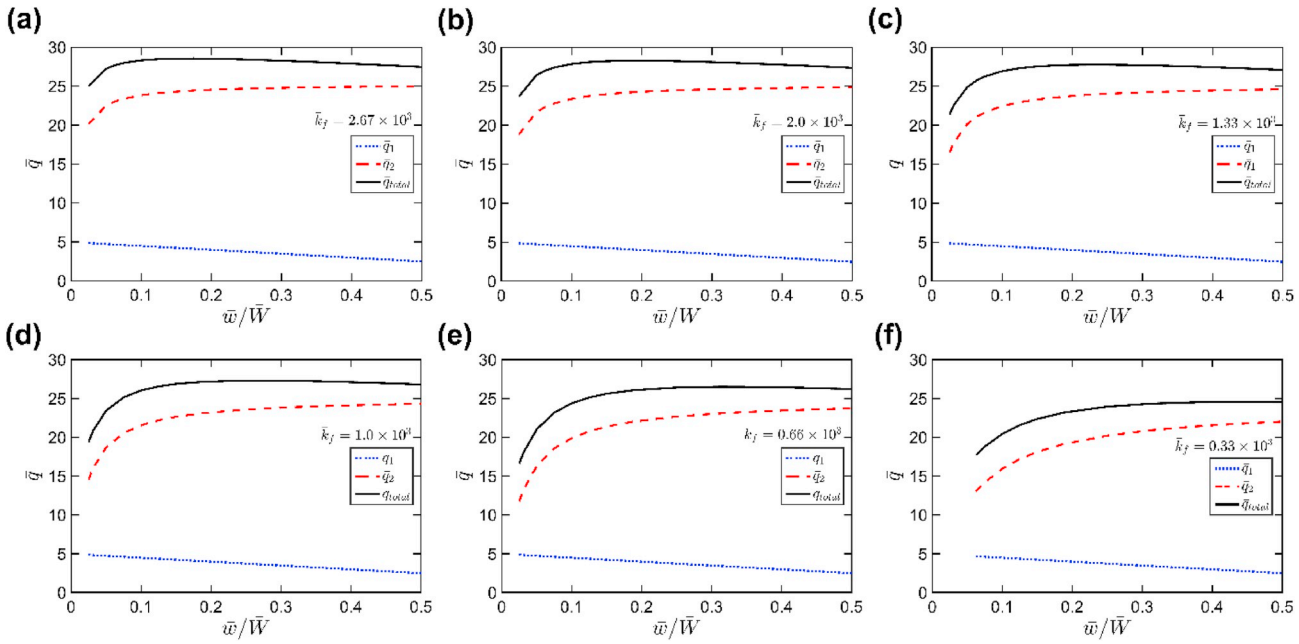

Fig. 6. Heat absorbed by the PCM up to $\bar{t} = 0.418$ as a function of fin size $\frac{\bar{w}}{\bar{W}}$ for six different fin thermal conductivities in transverse configuration with $\overline{W} = 2$, $\overline{L} = 4$, Ste $= 0.19$, $\bar{c}_f = 1.36$. Both components of heat absorbed are shown.

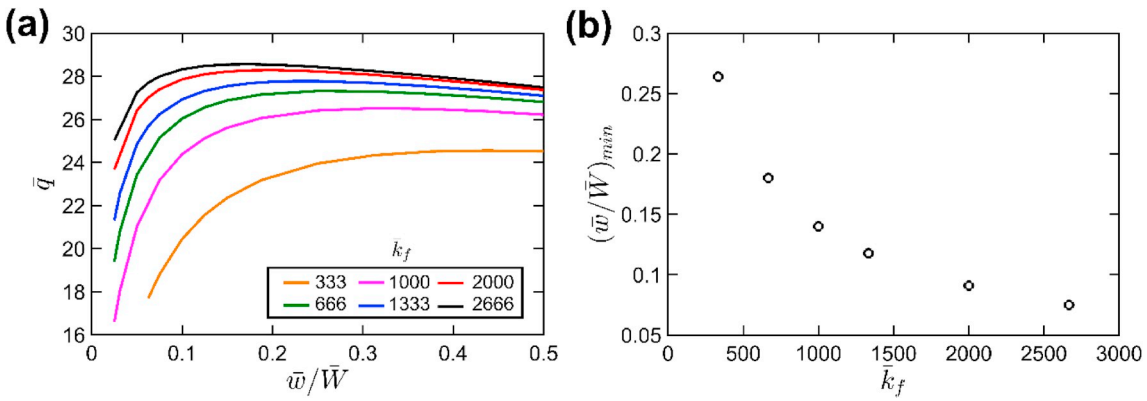

Fig. 7. (a) Plot of $\bar{q}_{total}$ up to $\bar{t} = 0.418$ as a function of fin size $\frac{\bar{w}}{\bar{W}}$ for different values of fin thermal conductivity for the case of transverse fin with $\overline{W} = 2$, $\overline{L} = 4$, Ste $= 0.19$,$\bar{c}_f = 1.36$; (b) Minimum value of $\frac{\bar{w}}{\bar{W}}$ needed to reach within 98% of the best possible heat absorbed, as a function of fin thermal conductivity.

the sum of $\bar{q}_1$ and $\bar{q}_2$, does not change considerably with fin width beyond a certain value of $\overline{w}/\overline{W}$. As a result, there is no thermal benefit in increasing the fin width beyond a minimum value. This clearly advocates for placing thin transverse fins.

Fig. 7(a) plots the total heat stored for all thermal conductivities on the same plot, and clearly shows, as expected, that the higher the fin thermal conductivity, the larger is the total heat absorbed in the PCM. Due to the saturation effect of $\overline{w}/\overline{W}$ on total heat stored, it is useful to define $(\overline{w}/\overline{W})_{min}$ as the value of $\overline{w}/\overline{W}$ that results in 98% of the maximum possible total heat stored. From a practical perspective, this may be viewed as the recommended fin size, beyond which, there is little additional thermal benefit. The dependence of $(\overline{w}/\overline{W})_{min}$ on fin thermal conductivity is shown in Fig. 7(b). This Figure shows a shift in the location of $(\overline{w}/\overline{W})_{min}$ towards lower values when thermal conductivity of the fin increases. This occurs because, as the fin thermal conductivity increases, the fin thermal resistance decreases, and therefore, fin temperature saturates at lower $((\overline{w}/\overline{W})_{min}$ values. Fig. 7(b) shows that improving fin thermal conductivity reduces the need for thick fin, but this effect does saturate quickly at high values of fin thermal conductivity. It is very important in practical fin design to consider the relationship between the peak stored energy, fin thermal conductivity and fin size, since selecting a thicker fin does not increase total stored energy.

Similar results for longitudinal fins are shown in Fig. 8. In the case of four equally distributed longitudinal fins, the total heat absorbed by the PCM does not change significantly with fin width ϕ_f. The heat transferred from fin to PCM, $\bar{q}_2$ remains nearly constant with ϕ_f, whereas $\bar{q}_1$ decreases linearly with ϕ_f as contact area between inner cylinder and the PCM decreases when fin size increases. This shows that even a very thin fin sufficiently promotes heat transfer. Therefore, fin insertion is important, but changes in fin size do not significantly affect thermal performance. Fig. 9 presents the dependence of total heat absorbed by the PCM on fin width for different longitudinal fin thermal conductivity values. This dependence is seen to be weaker than the transverse fin case.

While the total energy stored for the case of Cartesian fins has been shown to be highly dependent on fin size [28], Figures (6-9) show that the same is not the case for transverse or longitudinal fins. Nevertheless, fin insertion is still a very effective mechanism for increasing energy

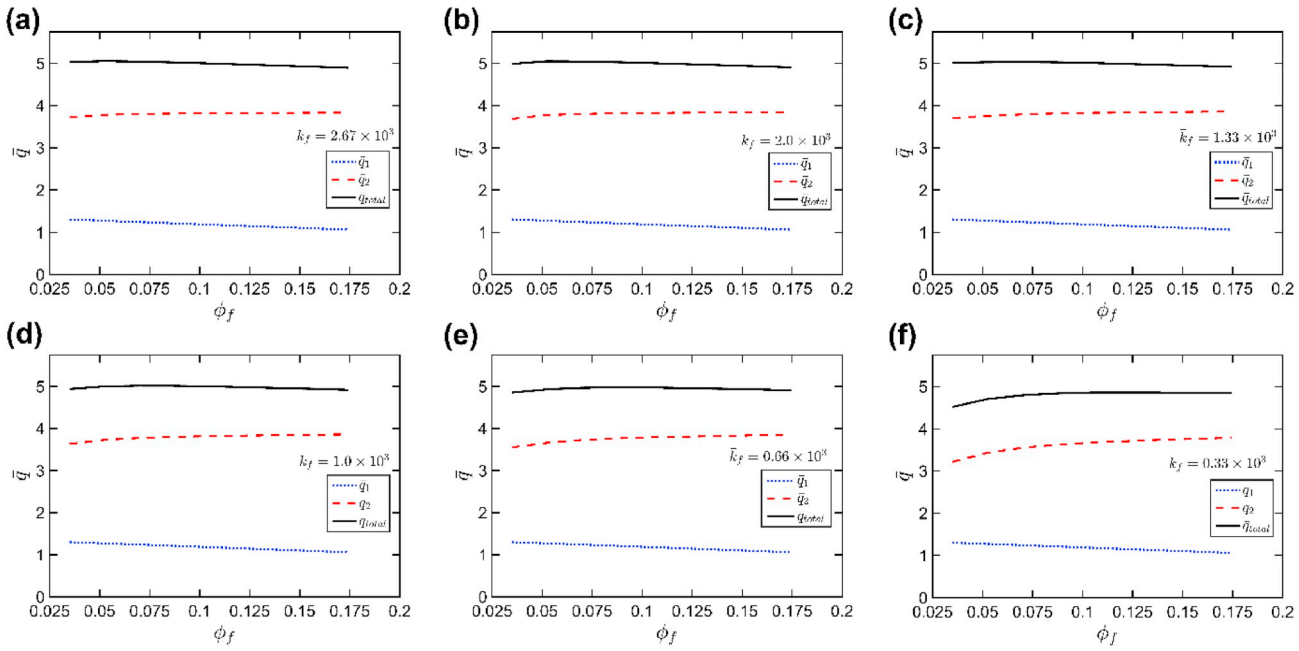

Fig. 8. Heat absorbed by the PCM up to $\bar{t} = 1.6722$ as a function of fin size ϕ_f for six different fin thermal conductivities in longitudinal configuration with $\phi_o = 0.7854$, $\bar{L} = 3$, Ste = 0.19, $\bar{c}_f = 1.36$. Both components of heat absorbed are shown.

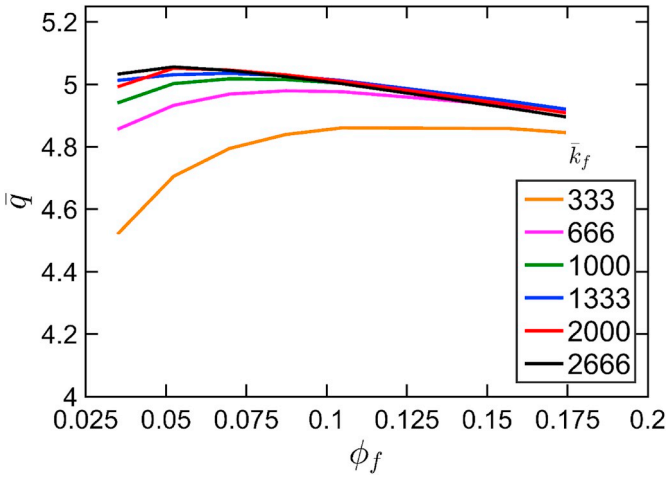

Fig. 9. Plot of $\bar{q}_{total}$ at $\bar{t} = 1.6722$ as a function of fin size ϕ_f for different values of fin thermal conductivity for the case of longitudinal fin with $\phi_o = 0.7854$, $\bar{L} = 3$, Ste = 0.19, $\bar{c}_f = 1.36$.

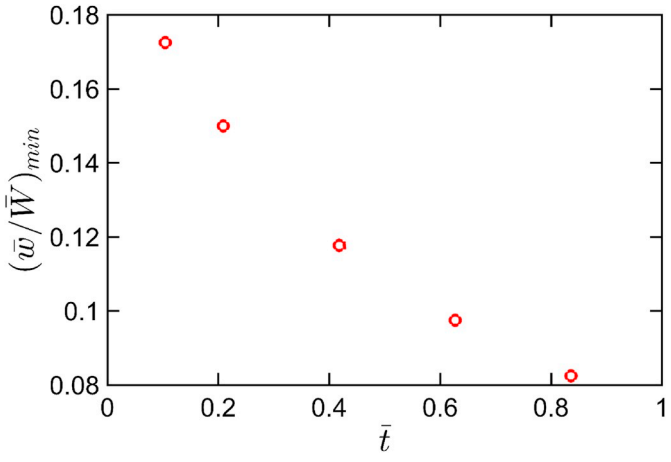

Fig. 10. Effect of total time available for heat transfer on the minimum fin width to reach within 98% of maximum possible heat stored for a transverse fin configuration, with $\overline{W} = 2$, $\bar{L} = 4$, Ste = 0.19, $\bar{k}_f = 1333$, $\bar{c}_f = 1.36$.

storage capability of cylindrical systems. Even with a thin fin, energy stored is much higher than no fin at all. However, choosing large-sized fins does not necessarily improve thermal performance. Inserting large fins may also not be attractive from the perspective of system weight and cost.

Typically fins are high thermal conductivity materials with $\bar{k}_f$ in the range of 333 up to 2666, with octadecane as the PCM. This work shows that in a system with transverse fins, the optimal fin size is almost independent of fin thermal conductivity for conductivities beyond 1500, as seen in Fig. 7(b). On the other hand, the optimal fin size depends strongly on fin thermal conductivity in the lower range of thermal conductivity. On the other hand, the maximum stored thermal energy in a system with longitudinal fins is not a strong function of fin size.

3.3. Effect of time available for heat transfer

Total time available for heat transfer in the system is a very important factor in determining effectiveness of the fin geometry. Clearly, the entire PCM will reach the wall temperature in the unlikely case of infinite time being available for heat transfer. In such a case, fin insertion is clearly counterproductive, since the presence of fins only reduces PCM volume, and consequently the total amount of energy stored. For most practical applications, where only a finite time is available, inserting fins is indeed beneficial. Fig. 10 presents variation in $(\overline{w}/\overline{W})_{min}$ with total heat transfer time for transverse fins. A similar trend has been reported for Cartesian fins [28]. Clearly, the larger the available time, the smaller is the fin width needed for heat transfer enhancement. As time passes, the role of the fin in providing extended surface and additional heat transfer pathway shrinks, and therefore, a larger fin becomes less and less attractive.

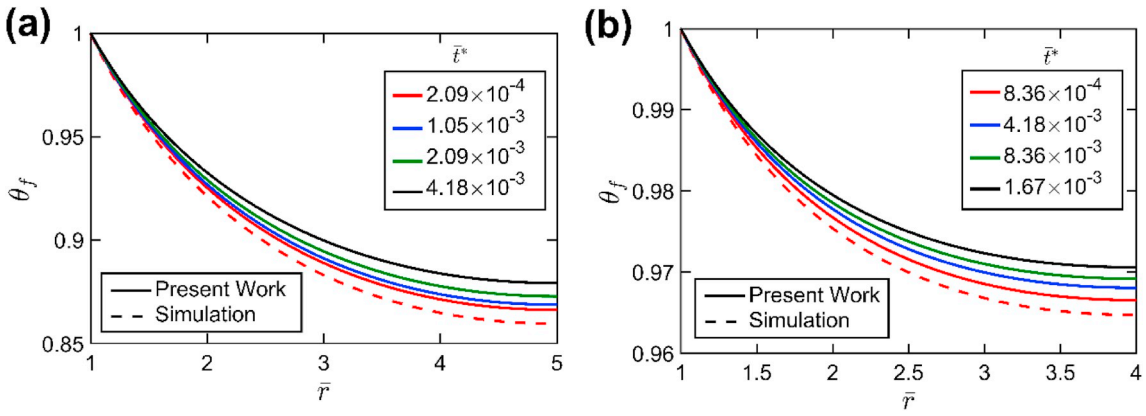

Fig. 11. Effect of $\bar{t}^*$ on the accuracy of computed temperature distribution for case of (a) transverse fin at $\bar{t} = 0.209$ and $\overline{W} = 2$, $\overline{w} = 0.5$,$\overline{L} = 4$, Ste $= 0.19$, $\overline{k}_f = 1580$, $\overline{c}_f = 1.36$ (b) longitudinal fin at $\bar{t} = 0.8361$ and $\phi_o = 0.7854$, $\overline{L} = 3$, Ste $= 0.19$, $\overline{c}_f = 1.36$. Results from finite-element simulation are also shown for comparison.

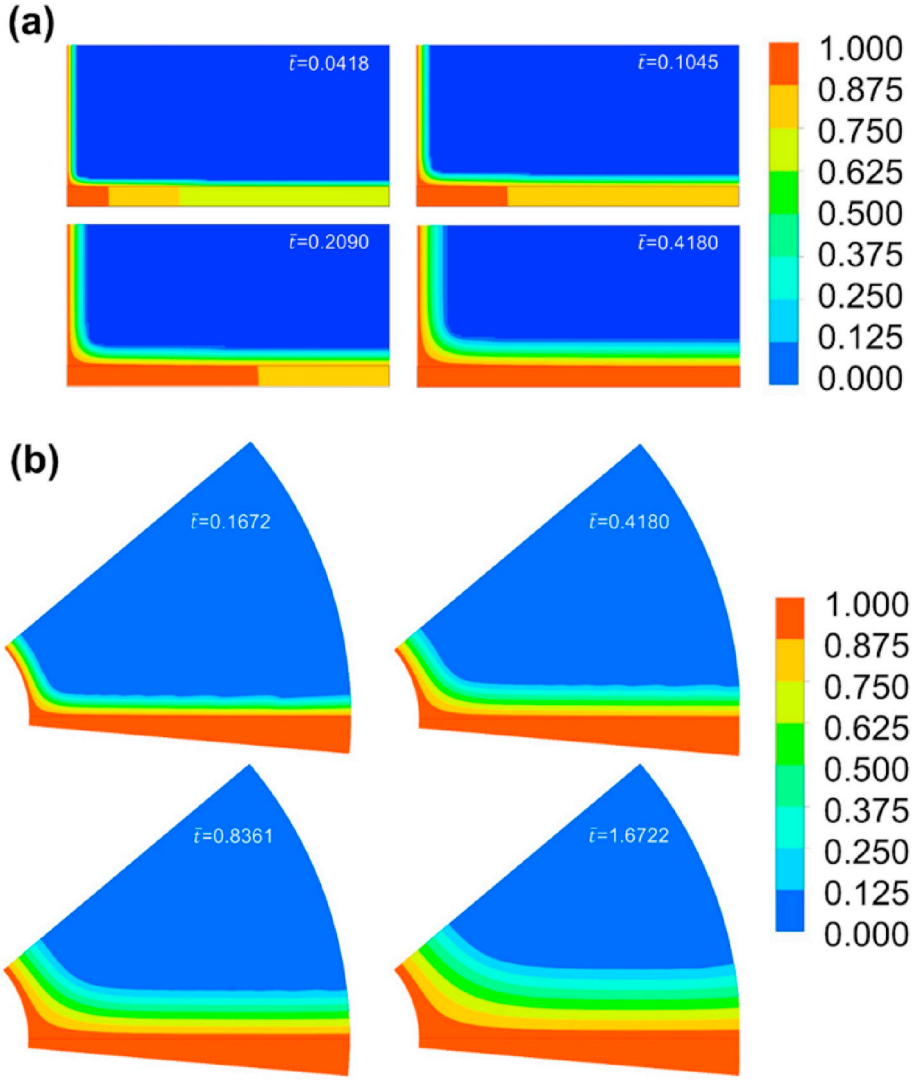

Fig. 12. Temperature colormap determined from finite-element simulations at different times for (a) transverse fin with $\overline{W} = 2$, $\overline{w} = 0.5$, $\overline{L} = 4$, Ste $= 0.19$, $\overline{k}_f = 1580$, $\overline{c}_f = 1.36$. and (b) longitudinal fin with $\phi_f = 0.087$, $\phi o = 0.7854$,$\overline{L} = 3$, Ste $= 0.19$,$\overline{k}_f = 1580$, $\overline{c}_f = 1.36$.

3.4. Effect of $\bar{t}^*$

As discussed in section 2.3, an approximation is used to initiate the time stepping process due to the singularity in equations (10) and (18) at $\bar{t} = 0$. This approximation ignores heat transfer into the PCM from the fin up to a short time $\bar{t}^*$. Clearly, the error introduced by this approximation must be understood, and a maximum tolerable value of $\bar{t}^*$ must be determined for a given acceptable error. Fig. 11(a) and (b) present fin temperature distribution for transverse and longitudinal configurations at $\bar{t} = 0.209$ and $\bar{t} = 0.8361$ respectively for multiple values of $\bar{t}^*$. For comparison, finite element simulation results are also presented. These Figures show that in both cases, the approximation error reduces as $\bar{t}^*$ decreases. These plots establish the maximum value of $\bar{t}^*$ for a given error level for a specific set of parameters.

A key assumption underlying the analysis presented here is that the two phase change fronts develop independent of each other, for both transverse and longitudinal fins. This assumption enables the independent determination of q_1 and q_2. In order to verify the validity of this assumption, fin and PCM temperature distributions are computed using finite-element simulations for both transverse and longitudinal fins. Temperature distributions for the two cases are shown in Fig. 12(a) and (b), respectively, at multiple times. Heat diffusion from inner cylindrical wall into the PCM, q_1, and heat diffusion from fin surface into the PCM, q_2, can be seen in the form of two independent phase change propagation fronts in these figures. Except for a small region close to the fin-wall interface, the two fronts do not interact much with each other. This justifies a key assumption behind the analysis in Section 2 that independently accounted for the contributions of the two fronts towards total energy stored.

4. Conclusions

The highly non-linear and transient nature of heat transfer in phase change energy storage systems presents formidable difficulties in theoretical analysis. This work presents a semi-analytical approach for solving this problem for transverse and longitudinal fins that are commonly used for heat transfer enhancement. Results show key similarities and differences between cylindrical fins and Cartesian fins studied in the recent past. For example, similar to Cartesian fins, it is shown that presence of fins increases thermal energy stored in the PCM significantly for both transverse and longitudinal fins for a given time. However, in contrast with Cartesian fins, the amount of stored energy is not a strong function of fin size. A key conclusion of the present work is that in general, even a thin fin provides excellent heat transfer enhancement, and that larger fins offer only diminishing returns. The underlying physics behind this process includes two conflicting effects of fin width on heat transfer components to the PCM, one indirectly through the fin and the other directly from the inner tube in contact with PCM were evaluated. The theoretical results presented here have several important practical applications. By quantifying the impact of fin geometry on heat transfer enhancement, the results presented here may help in geometrical optimization of phase change energy storage systems. The insights that even a small-sized fin results in significant benefit and that further increasing the fin size results in very little incremental benefit are both helpful for practical designers. The impact of available time window for heat transfer on the fin size is also an important consideration in practical designs.

Acknowledgments

This material is based upon work supported by CAREER Award No. CBET-1554183 from the National Science Foundation.

References

[1] U. Desideri, P.E. Campana, Analysis and comparison between a concentrating solar and a photovoltaic power plant, Appl. Energy 113 (2014) 422–433, https://doi.org/10.1016/j.apenergy.2013.07.046.
[2] U. Pelay, L. Luo, Y. Fan, D. Stitou, M. Rood, Thermal energy storage systems for concentrated solar power plants, Renew. Sustain. Energy Rev. 79 (2017) 82–100, https://doi.org/10.1016/j.rser.2017.03.139.
[3] A. Sharma, V. Tyagi, C. Chen, D. Buddhi, Review on thermal energy storage with phase change materials and applications, Renew. Sustain. Energy Rev. 13 (2009) 318–345, https://doi.org/10.1016/j.rser.2007.10.005.
[4] W.R. Humphries, E.I. Griggs, A Design Handbook for Phase Change Thermal Control and Energy Storage Devices, National Aeronautics and Space Administration, Scientific and Technical Information Office, Washington, 1977. NASA Technical Paper 1074.
[5] K.E. N'Tsoukpoe, H. Liu, N.L. Pierrès, L. Luo, A review on long-term sorption solar energy storage, Renew. Sustain. Energy Rev. 13 (2009) 2385–2396, https://doi.org/10.1016/j.rser.2009.05.008.
[6] J.M. Mahdi, S. Lohrasbi, E.C. Nsofor, Hybrid heat transfer enhancement for latent-heat thermal energy storage systems: a review, Int. J. Heat Mass Tran. 137 (2019) 630–649, https://doi.org/10.1016/j.ijheatmasstransfer.2019.03.111.
[7] Y. Tao, Y.-L. He, A review of phase change material and performance enhancement method for latent heat storage system, Renew. Sustain. Energy Rev. 93 (2018) 245–259, https://doi.org/10.1016/j.rser.2018.05.028.
[8] N.I. Ibrahim, F.A. Al-Sulaiman, S. Rahman, B.S. Yilbas, A.Z. Sahin, Heat transfer enhancement of phase change materials for thermal energy storage applications: a critical review, Renew. Sustain. Energy Rev. 74 (2017) 26–50, https://doi.org/10.1016/j.rser.2017.01.169.
[9] C. Ho, J. Gao, Preparation and thermophysical properties of nanoparticle-in-paraffin emulsion as phase change material, Int. Commun. Heat Mass Tran. 36 (2009) 467–470, https://doi.org/10.1016/j.icheatmasstransfer.2009.01.015.
[10] S.C. Lin, H.H. Al-Kayiem, Evaluation of copper nanoparticles – paraffin wax compositions for solar thermal energy storage, Sol. Energy 132 (2016) 267–278, https://doi.org/10.1016/j.solener.2016.03.004.
[11] K. Lafdi, O. Mesalhy, S. Shaikh, Experimental study on the influence of foam porosity and pore size on the melting of phase change materials, J. Appl. Phys. 102 (2007), 083549, https://doi.org/10.1063/1.2802183.
[12] D. Li, C. Yang, H. Yang, Experimental and numerical study of a tube-fin cool storage heat exchanger, Appl. Therm. Eng. 149 (2019) 712–722, https://doi.org/10.1016/j.applthermaleng.2018.12.024.
[13] R. Velraj, R. Seeniraj, B. Hafner, C. Faber, K. Schwarzer, Experimental analysis and numerical modelling of inward solidification on a finned vertical tube for a latent heat storage unit, Sol. Energy 60 (1997) 281–290, https://doi.org/10.1016/s0038-092x(96)00167-3.
[14] K. Ismail, J.r. Henríquez, L. Moura, M. Ganzarolli, Ice formation around isothermal radial finned tubes, Energy Convers. Manag. 41 (2000) 585–605, https://doi.org/10.1016/s0196-8904(99)00128-4.
[15] K. Ismail, C. Alves, M. Modesto, Numerical and experimental study on the solidification of PCM around a vertical axially finned isothermal cylinder, Appl. Therm. Eng. 21 (2001) 53–77, https://doi.org/10.1016/s1359-4311(00)00002-8.
[16] W. Ogoh, D. Groulx, Effects of the number and distribution of fins on the storage characteristics of a cylindrical latent heat energy storage system: a numerical study, Heat Mass Tran. 48 (2012) 1825–1835, https://doi.org/10.1007/s00231-012-1029-3.
[17] C. Liu, D. Groulx, Experimental study of the phase change heat transfer inside a horizontal cylindrical latent heat energy storage system, Int. J. Therm. Sci. 82 (2014) 100–110, https://doi.org/10.1016/j.ijthermalsci.2014.03.014.
[18] R.E. Murray, D. Groulx, Experimental study of the phase change and energy characteristics inside a cylindrical latent heat energy storage system: Part 1 consecutive charging and discharging, Renew. Energy 62 (2014) 571–581, https://doi.org/10.1016/j.renene.2013.08.007.
[19] M. Kabbara, D. Groulx, A. Joseph, Experimental investigations of a latent heat energy storage unit using finned tubes, Appl. Therm. Eng. 101 (2016) 601–611, https://doi.org/10.1016/j.applthermaleng.2015.12.080.
[20] Y. Kozak, T. Rozenfeld, G. Ziskind, Close-contact melting in vertical annular enclosures with a non-isothermal base: theoretical modeling and application to thermal storage, Int. J. Heat Mass Tran. 72 (2014) 114–127, https://doi.org/10.1016/j.ijheatmasstransfer.2013.12.058.
[21] T. Rozenfeld, Y. Kozak, R. Hayat, G. Ziskind, Close-contact melting in a horizontal cylindrical enclosure with longitudinal plate fins: demonstration, modeling and application to thermal storage, Int. J. Heat Mass Tran. 86 (2015) 465–477, https://doi.org/10.1016/j.ijheatmasstransfer.2015.02.064.
[22] A. Rozenfeld, Y. Kozak, T. Rozenfeld, G. Ziskind, Experimental demonstration, modeling and analysis of a novel latent-heat thermal energy storage unit with a helical fin, Int. J. Heat Mass Tran. 110 (2017) 692–709, https://doi.org/10.1016/j.ijheatmasstransfer.2017.03.020.
[23] A. Erek, Z. Ilken, M.A. Acar, Experimental and numerical investigation of thermal energy storage with a finned tube, Int. J. Energy Res. 29 (2005) 283–301, https://doi.org/10.1002/er.1057.
[24] W.-W. Wang, L.-B. Wang, Y.-L. He, Parameter effect of a phase change thermal energy storage unit with one shell and one finned tube on its energy efficiency ratio and heat storage rate, Appl. Therm. Eng. 93 (2016) 50–60, https://doi.org/10.1016/j.applthermaleng.2015.08.108.
[25] A.A. Al-Abidi, S. Mat, K. Sopian, M. Sulaiman, A.T. Mohammad, Internal and external fin heat transfer enhancement technique for latent heat thermal energy

storage in triplex tube heat exchangers, Appl. Therm. Eng. 53 (2013) 147–156, https://doi.org/10.1016/j.applthermaleng.2013.01.011.
[26] A.A. Al-Abidi, S. Mat, K. Sopian, M. Sulaiman, A.T. Mohammad, Numerical study of PCM solidification in a triplex tube heat exchanger with internal and external fins, Int. J. Heat Mass Tran. 61 (2013) 684–695, https://doi.org/10.1016/j.ijheatmasstransfer.2013.02.030.
[27] Z. Liu, X. Sun, C. Ma, Experimental investigations on the characteristics of melting processes of stearic acid in an annulus and its thermal conductivity enhancement by fins, Energy Convers. Manag. 46 (2005) 959–969, https://doi.org/10.1016/j.enconman.2004.05.012.
[28] A. Mostafavi, M. Parhizi, A. Jain, Theoretical modeling and optimization of fin-based enhancement of heat transfer into a phase change material, Int. J. Heat Mass Transf. Int. J. Heat Mass Transf. 145 (2019) 1–10, https://doi.org/10.1016/j.ijheatmasstransfer.2019.118698, 118698.
[29] P. Lamberg, K. Sirén, Approximate analytical model for solidification in a finite PCM storage with internal fins, Appl. Math. Model. 27 (2003) 491–513, https://doi.org/10.1016/s0307-904x(03)00080-5.
[30] P. Lamberg, Approximate analytical model for two-phase solidification problem in a finned phase-change material storage, Appl. Energy 77 (2004) 131–152, https://doi.org/10.1016/s0306-2619(03)00106-5.
[31] P. Lamberg, K. Sirén, Analytical model for melting in a semi-infinite PCM storage with an internal fin, Heat Mass Tran. 39 (2003) 167–176, https://doi.org/10.1007/s00231-002-0291-1.
[32] V. Shatikian, G. Ziskind, R. Letan, Numerical investigation of a PCM-based heat sink with internal fins, Int. J. Heat Mass Tran. 48 (2005) 3689–3706, https://doi.org/10.1016/j.ijheatmasstransfer.2004.10.042.
[33] K.A. Rathjen, L.M. Jiji, Heat conduction with melting or freezing in a corner, J. Heat Tran. 93 (1971) 101, https://doi.org/10.1115/1.3449740.
[34] M. Parhizi, A. Jain, The impact of thermal properties on performance of phase change based energy storage systems, Appl. Therm. Eng. 162 (2019) 1–10, https://doi.org/10.1016/j.applthermaleng.2019.114154, 114154.
[35] J. Caldwell, Y. Kwan, On the perturbation method for the Stefan problem with time-dependent boundary conditions, Int. J. Heat Mass Tran. 46 (2003) 1497–1501, https://doi.org/10.1016/s0017-9310(02)00415-5.
[36] G. Lock, J. Gunderson, D. Quon, J. Donnelly, A study of one-dimensional ice formation with particular reference to periodic growth and decay, Int. J. Heat Mass Tran. 12 (1969) 1343–1352, https://doi.org/10.1016/0017-9310(69)90021-0.
[37] N.R. Jankowski, F.P. McCluskey, A review of phase change materials for vehicle component thermal buffering, Appl. Energy 113 (2014) 1525–1561, https://doi.org/10.1016/j.apenergy.2013.08.026.
[38] K. Sasaguchi, H. Imura, H. Furusho, Heat transfer characteristics of a latent heat storage unit with a finned tube (Experimental studies on solidification and melting processes), Bull. JSME 29 (1986) 2978–2985.